Reducing direct exposure to exhaled aerosol through a portable desktop fan

ATMOSPHERIC ENVIRONMENT: X 22 (2024) 100263

Contents lists available at ScienceDirect

Atmospheric Environment: X

journal homepage: www.journals.elsevier.com/atmospheric-environment-x

Reducing direct exposure to exhaled aerosol through a portable desktop fan

Hamed Rasam, Vincenzo Maria Gentile *, Paolo Tronville, Marco Simonetti

Deparment of Energy, Politecnico di Torino, C.so Duca degli Abruzzi 24, 10129, Italy

ARTICLE INFO

Keywords:
Desktop fan
V-shape air blades
Local airflow control
Proximity transmission
CFD
COVID-19
Aerodynamic confinement

ABSTRACT

Vulnerable individuals close to infected people emitting a respiratory cloud containing infectious load can inhale a pathogen dose, experiencing a more severe impact on their health compared to other individuals breathing the mixed air in the same room. In crowded spaces, this issue is crucial. Employing local airflow patterns can reduce the proximity risk of inhalation and subsequent transmission across short distances. This study proposes an experimental and numerical analysis of a novel personal and portable device creating a short-range air barrier to transmitting airborne pathogens in proximity. The portable device adopts V-shaped air blades affecting the trajectory of the particle-laden respiratory cloud emitted by the respiratory system of the infected individual. Experimental results, supported by CFD analysis, indicate that controlling local airflow through the V-shaped jet significantly reduces local particle concentrations by more than 60%, compared to typical scenarios without a local airflow control.

1. Introduction

The COVID-19 pandemic has increased the attention to health risks associated with airborne contaminants and poor indoor air quality (Baboli et al., 2021), (Anderson et al., 2020). Particles emitted by the respiratory system evaporate quickly and generate aerosols. Thanks to the long time airborne particles remain suspended, people get easily exposed to pathogens (Jensen, 2020) (Tang et al., 2021; Liu et al., 2017a, 2017b; Jia et al., 2022). The presence of an infected occupant in an indoor environment forces the people around him to withstand the infectious aerosol emitted by his respiratory system, directly or indirectly (Nair et al., 2022; Azuma et al., 2020; Bourouiba, 2020; Jayaweera et al., 2020; Xu et al., 2022a; Merhi et al., 2022).

Ventilation systems and indoor airflow topology can effectively mitigate the spread of pathogens, reducing the exposure of vulnerable persons to infectious doses by direct and indirect mechanisms (Eilts et al., 2021; Melikov, 2020; Cortellessa et al., 2023). Dilution through ventilation and air filtration are common practices to reduce the concentration of indoor airborne particles (Pistochini et al., 2022; Li and Tang, 2021; Gettings et al., 2021; Christopherson et al., 2020). A minimum recommended 7–10 L/s outdoor airflow rate per person is recommended (Bourouiba, 2021). This value increases to 15 L/s per person in specific circumstances, such as environments with the risk of tuberculosis transmission (Morey, 1994). When dealing with COVID-19, both the Center for Disease Control and Prevention (CDC) (Center for Disease Control and Prevention, 2019) and the World Health Organization (WHO) (World Health Organization, 2021) require a ventilation rate of 160 l/s/patient or at least 12 air changes per hour (ACH) in critical areas such as the Intensive Care Units (ICU). They also recommend the control of airflow patterns.

However, mechanical ventilation systems optimized for indoor environments seldom exceed 10 ACH (Bourouiba, 2021).

Estimating ACH is crucial for occupancy assessment but is not the only key aspect. The indoor airflow pattern, impacting infective aerosol advection, can lead to non-homogeneous aerosol distribution within the space. Achieving perfect air mixing in populated areas is challenging when employing mixing ventilation. The formation of regions with higher particle concentrations due to airflow recirculation (Linden, 1999; Zhang et al., 2020; Yuan et al., 1998; Shan et al., 2016; Bhagat et al., 2020) is a risk. On the other hand, displacement ventilation may offer more favorable conditions for the occupants. Indeed, when a stable transitional layer occurs, the contaminated upper layer can be separated from the lower area, creating a cleaner respiratory area and reducing occupant disease transmission risks (Wachenfeldt et al., 2007), (Hashimoto and Yoneda, 2009).

A similar effect of dilution of airborne pathogens can be achieved by cleaning the air with centralized mechanical systems or portable room air cleaners (Kelly and Fussell, 2019), (Morawska et al., 2020).

However, although mechanical ventilation effectively decreases indirect exposure by diluting indoor aerosol concentrations and renewing

* Corresponding author.
E-mail address: vincenzo.gentile@polito.it (V.M. Gentile).

https://doi.org/10.1016/j.aeaoa.2024.100263
Received 30 January 2024; Received in revised form 26 April 2024; Accepted 2 May 2024
Available online 8 May 2024

indoor air, its effectiveness against direct exposure is limited. If vulnerable individuals are close to an infectious aerosol source, the general ventilation system cannot control locally the airflow, thus potentially failing to prevent the fast spread of infectious particles near the infecting person (Liu et al., 2017a), (Chen et al., 2020), (Ai and Melikov, 2018).

In such cases, besides using protective masks for source control, preventing direct exposure to airborne particles is a crucial strategy to limit the transmission of respiratory viruses. (Bourouiba, 2021), (Chen et al., 2020), (Mikszewski et al., 2022). For example, the interposition of physical barriers reduces the direct transmission, intercepting the droplet flow and mitigating the occupants' infection risk (Chan et al., 2020; Ye et al., 2021; Ahmadzadeh and Shams, 2022; Ren et al., 2021; Mirzaie et al., 2021).

Personalized airflow control is an effective tool investigated by researchers. Personalized Ventilation (PV) technologies, such as air curtains (Ma et al., 2022; Chen et al., 2021; Xu et al., 2022b; Mboreha et al., 2022), directional jets (Xu et al., 2020), and portable air purifiers (Zhao et al., 2020), are the most common solutions.

The scientific literature about the effectiveness of portable air purifiers, specifically used to reduce the direct contagion route, is extensive. These devices demonstrate their effectiveness as fast, deployable, and moderately cheap solutions (Cooper et al., 2022; Grinshpun et al., 2005; V Abhijith et al., 2022). Portable air purifier use has been associated with a wide range of infection risk reduction, from less than 10% to almost 90% on average in various indoor settings (Shen et al., 2021). The environment where the air purifiers operate considerably impacts their performance (Burgmann and Janoske, 2021; Curtius et al., 2021; Tobisch et al., 2021). Additionally, they can induce an airflow topology that can alter the distribution of particles in the room because air purifiers generate high-momentum jets, potentially negatively affecting the occupants (Ham, 2020). Hence, it is vital to evaluate the correct position of air purifiers before using them.

PV is frequently used in vehicles (such as automobiles and aircraft) to increase the comfort of travelers (Gao and Niu, 2008), (Ružić and Časnji, 2011). A PV of 10 L/s and a centralized mixing ventilation system could significantly improve air quality with a maximum exposure reduction of pollutants of 97% (Al Assaad et al., 2021). Recent studies demonstrated that PV is a promising approach for short-distance airborne infection management, reducing bio-aerosol deposition on the face and the body and inhalation by up to 98%, 85%, and 100%, respectively (Xu et al., 2021).

However, all these solutions have drawbacks. PV requires specific ducting, which restricts its use to locations with favorable conditions. On the other hand, even though portable purifiers are ductless, they need appropriate filter management. If the air filter efficiency is high enough and does not drop off during its service life, its pressure drop associated with an adequate airflow rate may require a powerful and noisy fan while increasing energy use ("RESIDENTIAL AIR CLEANERS A Technical).

In the existing literature, extensive research has been conducted on various ventilation strategies aimed at mitigating the transmission of airborne pathogens within indoor environments. However, there is a notable gap in studies focusing on short-range ventilation strategies that modify airflow patterns without relying on personalized ventilation (PV) or air purifier systems. While prior investigations often involve the placement of blowers in close proximity to occupants to reduce airborne transmission risks, these approaches typically incorporate either the introduction of fresh air through PV or the use of filtering systems to decrease aerosol concentration. This gap highlights the need for research exploring alternative methods for short-range airflow control, which could provide valuable insights into novel approaches for minimizing the spread of respiratory viruses indoors.

1.1. Objectives

Innovative technological solutions are essential in addressing the challenge of transmission of airborne pathogens indoors. The limitations of centralized mechanical ventilation systems hinder effective short-distance transmission risk mitigation for vulnerable individuals. Alternative localized solutions for controlling airflow near the occupants are suitable, especially if they do not require adaptation to systems and buildings. Our investigation focuses on generating inertial control over particle motion to minimize the risk of direct transmission, diverging from conventional blowers by targeting airflow patterns in close proximity to individuals. Specifically, we explore alternatives such as air blades to create a barrier effect and air suction to redirect exhaled particles. To meet the study's simplicity constraint, we emphasize solutions like the device employing air blades, which aligns with our aim to provide a deployable and effective approach for separating occupants.

We present the results obtained employing a prototype of a novel personal device that works on the close direct exposure range. It consists of a desktop fan generating V-shaped air blades acting as a short-range aerodynamic barrier for exhaled aerosol particles. The device controls the local airflow without requiring outdoor air or air cleaners. Its goal is to reduce the risk of contagion without the drawbacks of more complex solutions. The device design aims to provide a safer region among people in crowded environments with a simple deployable solution. We provide an integrated strategy to evaluate the effectiveness of the desktop fan at short distances in reducing particle concentration. We excluded any centralized ventilation effect to assess the device performance more precisely. The detailed description of the device and its integration into the study are described in Section 2.1. We conducted the sensitivity study using the Computational Fluid Dynamic (CFD) STAR-CCM + code.

2. Methodology

We consider the methodology divided into three sections. Firstly, an experimental assessment investigated the impact of V-shaped air blades generated with a 3D-printed desktop fan on mitigating the transmission of exhaled aerosol particles in a crowded environment. A controlled environment simulated a gathering scenario with a mannequin head emitting airborne particles. An optical particle spectrometer measured the particle concentration and distribution with and without the desktop fan, assessing its impact.

Secondly, the Star-CCM + CFD software modeled the experimental scenario, enabling the tracking of particle trajectories. Data evaluation enabled the study of the V-shaped air blades on air velocity and airflow topology around the occupants.

Finally, we used an efficacy parameter to compare experimental data and CFD modeling results. This parameter serves as a quantitative metric to assess the agreement and effectiveness of both approaches in addressing the mitigation of airborne particle transmission. By integrating experimental data with computational simulations, this study provides valuable insights into the potential application of V-shaped desktop fans to mitigate the risk of airborne infection transmission in crowded environments.

2.1. Experimental setup and testing procedure

A desktop portable fan generates 90° V-shaped air blades, designed to establish individual safe zones in spaces where face masks may not be practical, such as restaurants. As shown in Fig. 1, this device aims to create an individual safer zone with minimized viral interaction while remaining connected to the rest of the group. Fig. 1b and c shows the two-dimensional schematics of the desktop portable fan.

The form comprises a light main body, propped over the table by a base. The main body acts like a plenum by which 12 miniature, low-consumption 5-W fans, mounted in racks of 3 on each side of the cube, blow air to form the air blades. The air enters the main body

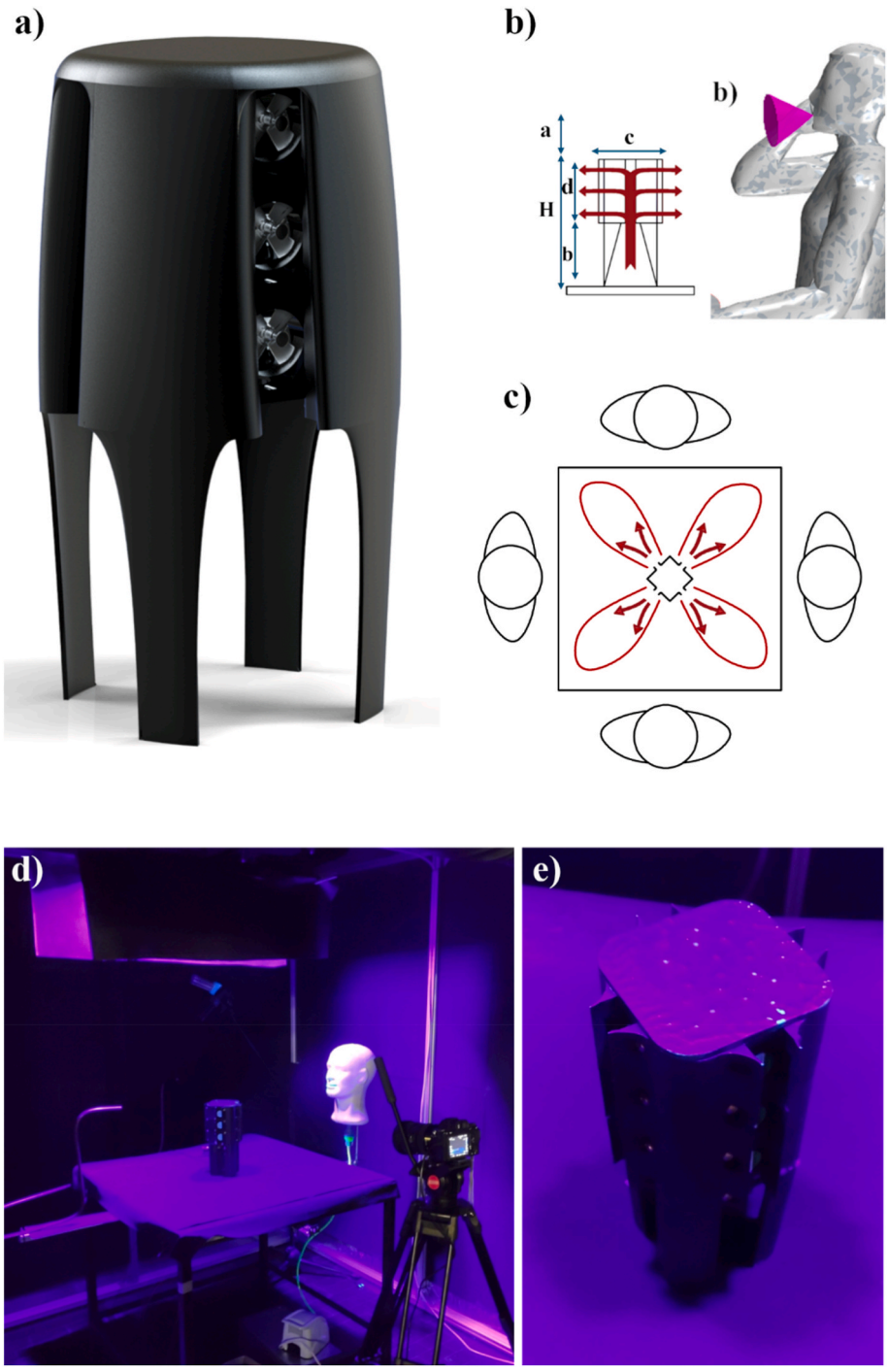

Fig. 1. a) 3D render of the portable and personal device (solid size: 0.10m × 0.10m × 0.25m) generating the V-shaped air blades, which is 3D printable. b) Side view and schematic representation of the air movement: air enters the main body or plenum through the base (a = distance from mouth to the top of device, b = distance from the bottom of the device to the table, c = width of the device, d = body height of the device and H = distance from top of the device to the table). c) Top view and schematic representation of the air movement: the device positioned in the center of a table can confine the susceptible area of each individual. d) Experimental setup including a mannequin head, the V-shaped air blades generator, a liquid aerosol generator connected to the mannequin head, the copper sampling probes located opposite to the aerosol source, a professional camera for side view imaging, two UV light source for fluoroscopy visualization of the contrast aerosol. e) Magnification of the 3D-printed personal ventilation device that generates the V-shaped air blades effect.

through the base. The V-shaped air blades generate a natural barrier to virus-laden aerosols by being positioned obliquely on the table. This device operates without cleaning the air over a short distance.

The experimental setup goal is to quantify the effect of the V-shaped air blades in a quasi-realistic environment without any additional ventilation. The case study considers two people facing each other at a restaurant table while a generic micrometer-scale liquid aerosol generator simulated particle emissions from the respiratory tract of the infected person.

In a normal indoor setting, detecting infected particles emitted by a person during breathing and speaking is challenging due to the high background concentration of ambient particulate matter (PM), and typical tests require a clean room environment (Chao and Wan, 2006), (Shao et al., 2020). A simpler but less conventional and alternative

approach can be generating an aerosol jet with a particle concentration one order of magnitude higher than typical human respiratory emissions, allowing clear detection and visualization against the background. This study used the second approach to test the device's performance. The rationale behind employing a significantly heightened concentration involves simulating worst-case scenarios resembling super-spreading events (Morawska and Buonanno, 2021), (Miller et al., 2021), thereby providing a robust test of the device's performance under extreme but plausible conditions. This methodology is supported by aerosol physics principles, suggesting that such an increase in concentration should not materially affect the core dynamics of particle interactions, including coagulation, within the short timescales of our experiments Supplementary Information section 1(SI1) (Kulkarni et al., 2011), (Park et al., 1999). The hypothesis underlying this testing condition is that such a high concentration does not significantly alter particle interactions or the advection mechanism induced by the fan. Consequently, the local effects of air blades on the aerosol jet with higher particle numbers remain comparable to those observed on a jet with fewer particles (Hinds, 1999). It is important to recognize the assumptions underlying this approach: while increasing the particle concentration provides a stringent testing environment, it assumes the absence of significant deviations in particle dynamics at these elevated concentrations. This method, chosen for its practicality in simulating high-risk exposure scenarios, is predicated on a careful extrapolation of aerosol physics, aiming to ensure the reliability of detection in controlled settings without substantially altering particle behavior.

The testing environment was a dark chamber (3x3x3 m) covered with light-absorbent foils, characterized by a Lambertian behavior, to reduce as much as possible direct light reflectance (Fig. 1d and e). We aerosolized a fluorescent liquid. Two UV LEDs (80 W, wavelength 385–400 nm, aperture angle of the light beam 120°) generated the contrast to visualize the liquid particles. We employed a professional camera to capture the particle behavior. In the dark room, on two opposite sides of a (0.8 × 0.8 m) table, we attached a mannequin head to the aerosol generator on one side and a probe on the other. The mannequin head replicated the human mouth and nose emissions. The desktop fan located in the middle of the table while a = 10 cm. The probe comprised a copper pipe (diameter 0.008 m) and was connected to a TSI 3330 Optical Particle Sizer (OPS) (Li et al., 2022), measuring airborne particles within the 0.3–10 μm range. A conductive silicon pipe connected the probe to the OPS, minimizing particle losses caused by electrostatic charges (Yu et al., 2009). To address and quantify potential losses attributable to tubing, our approach incorporated a detailed theoretical analysis, examining loss mechanisms such as inertial impaction, diffusion, turbulent mixing, and the influence of tubing bends, in line with established aerosol physics principles as discussed by (Kulkarni et al., 2011), (Hinds, 1999). The results of this comprehensive evaluation, detailing the minimal yet quantifiable losses for each particle size bin through different aforementioned mechanisms, are presented in (SI2). Although these uncertainties are exceptionally low for each particle size bin, it's important to recognize that they introduce an additional layer of uncertainty to our measurements. As such, these calculated losses could be added to the measurement uncertainty for each size bin, ensuring our analysis remains as accurate and transparent as possible. This careful consideration of tubing losses, even though minor, underscores our commitment to methodological rigor and the reliability of our findings.

The testing procedure allowed the comparison of the aerosol transmission from the emitting source to the sampling probe, with and without the V-shaped air blades generated by the personal fan device.

Each experiment was carried out for 300 s and repeated five times. During each interval between tests, we opened the air vents. An exhaust fan, mounted with a HEPA filter, removed the previously emitted fluorescent liquid particles still floating in the air inside the room.

During the overall test duration (300 s), for the first 30 s the generator device remained inactive, and the background concentration was measured, then active for 15 s activation, and again turned off for the remaining time (255 s). Throughout the test period, the mannequin head, which served as a proxy for the infected individual placed at one side of the table, released fluorescent aerosol particles into the air through two nasal and one oral outlet. On the other side of the table, the copper pipe probe was located within the volume representative of a susceptible subject. The OPS device counted particles over a 30-s timespan and logged the fluctuation of the aerosol during the entire 300-s test trial. The OPS sizes particles over 12 size channels within the 0.3–10 μm range (Morawska et al., 2009), (Johnson et al., 2011). Fig. 3 reports the test results with and without the V-shaped air blades.

Table 1
Main characteristics of the instruments used during the experiments.

Measurement instrument	Functionality	Measurement range	Error
TSI OPS 3330	Particle counting and sizing	0.3–10 μm	<5% (size)
Hotwire anemometer Testo 405i	Air velocity	0–30 m/s	<5%
Testo 440 dp	Turbulence intensity	0–100%	<1.5%

Testo 405i and 440dp instruments (Table 1) measured the velocity field generated by the V-shaped air blades at each of the four outlet sections. We divided each outlet section (2 × 12.5 cm) into three columns and nine rows. Sensors measured each grid node's average velocity and turbulence intensity over 1 min. We repeated the procedure three times for each node and each outlet section. Fig. 4 reports the velocity measurements and SI 7 represents the turbulence intensity measurements.

2.2. CFD modeling

A Computational Fluid Dynamics (CFD) model replicated the scenario of the experimental setup. We simulated the trajectory of the exhaled droplets in a host-to-host configuration and stagnated air conditions of the simulated indoor environment.

The numerical characterization of the velocity, pressure, and temperature fields and the motion and interaction between the droplets and the fluid was carried out using the Star-CCM + software. We modeled the droplet dynamic with a Lagrangian multiphase approach based on a dispersed dilute two-phase flow. The Eulerian-Lagrangian method solves the continuum equations for the airflow (continuous phase) and Newton's equation of individual droplet motion. This method is particularly suitable for this study because the spacing between droplets in the exhausted air plume is sufficiently large, and the volume percentage of the droplets is low enough ($<10^{-3}$) (Cortellessa et al., 2021).

Particles generated in the simulation are spherical, with a density of 1000 kg/m^3, log-normal particle size distribution (Morawska et al., 2009), (Johnson et al., 2011) within 0.3–10 μm (geometric mean size diameter 1.32 μm, and geometric standard deviation 2.04 μm). The SIMPLE solution algorithm, with a time step of 0.1 s, solved the transient equations of the problem.

We did not model the buoyancy-driven human thermal plume (Bayram and Korobenko, 2022). Neglecting the human thermal emission corresponds to a conservative scenario for the goal of this work, as the thermal plume can act as an air curtain to protect the person from the penetration of airflow exhaled by other people (Wei and Li, 2016). Other studies observed that the thermal plume can increase the exposure to particles generated near the floor, entrained in the human thermal plume boundary layer, and transported upward to the inhalation area of the subject (Sun et al., 2021). In contrast, our study positioned the primary particle source, the emitter's mouth, at the same height as the receiving individual's nostrils and mouth. In addition, given the rapid evaporation of droplets smaller than 50 μm (Cortellessa et al., 2021), (Xie et al., 2007), (Chen and Zhao, 2010), we have excluded the

Table 2
Solver and physics model (Sheikhnejad et al., 2022) and B.C used in the simulation.

Model	Particle tracking	Background airflow	Space	Time	Flow	Viscous Regime
	Lagrangian	Eulerian	3-Dimension	Implicit unsteady	Segregated	Turbulent K-Omega
Model	**Particle-air interaction**	**Particle wall impingement**	**Drag force Coefficient**	**Equation of State**	**Transition**	**Near-wall treatment**
	Two-way coupling	Bai-Gosman	Schiller-Naumann	Constant density	Gamma	SST-k-ω
B.C	**V-shaped air blades outlet velocity**	**V-shaped air blades inlet gauge pressure**	**Exhaled air plume initial velocity** (Chen et al., 2020)	**Room Temperature**	**Initial room pressure**	**Airborne particle Temperature**
	1.5–5 m/s	0 Pa	5 m/s	25 °C	1 atm	37 °C

transient process from droplet to droplet nucleus in our CFD simulations (Bayram and Korobenko, 2022), (He et al., 2011; Seepana and Lai, 2012; Yang et al., 2018; Liu et al., 2020; Kang et al., 2015). Our study primarily focuses on post-evaporation particle transfer, as it aligns with our goal of understanding the advective effectiveness of V-shaped air blades.

Furthermore, the Eulerian-Lagrangian numerical model was used to track particles during their path in the room. The particles reaching the mouth and nostril surfaces of the susceptible subject were considered and counted for the efficiency evaluation (Gallo et al., 2021), as reported in the following section. Table 2 list the boundary condition (B.C) values, the physics, and the solver models. It's worth noting that the models used in Table 2 are fully justified in reference (Sheikhnejad et al., 2022), a technical paper specifically addressing this subject.

2.2.1. Geometry

The distribution of droplets at close distances has been studied using the Eulerian-Lagrangian model. As shown in Fig. 2a, the geometry considered for this investigation consists of two identically sized individuals seated 0.80 m apart on a table while a = 15 cm, d = 12 cm, and b = 25 cm, resulting in a total distance from the mouth to the table surface a + H = 52 cm. One individual is an emitter who exhales through the nasal and oral airways of the respiratory tract, represented by two cone-shaped injectors (Fig. 2b and c). The other individual is a vulnerable participant seated on the other side of the table and immersed in the airborne particles jet. The V-shaped air blades generator is placed at the center of the table.

2.2.2. Mesh

In our CFD simulations, a sophisticated meshing approach was utilized to ensure both computational efficiency and accuracy. The process began with the Surface Remesher, which created a detailed surface mesh crucial for accurately capturing the geometry. Any inconsistencies found were corrected by the Automatic Surface Repair, providing a robust foundation for subsequent meshing. Adaptive mesh refinement was then achieved through the Geometric Sensitivity model, which enhanced the mesh in critical areas based on geometric complexity. At the heart of our volume meshing strategy was the Polyhedral Mesher, selected for its ability to deliver detailed results without an excessive computational burden, effectively reducing the element count while maintaining accuracy. Addressing the specific challenges of meshing narrow spaces, the Thin Mesher ensured efficient and precise meshing, and the Prism Layer Mesher was instrumental in accurately capturing boundary layer effects near surfaces—a key aspect of aerosol dynamics (Cd-Adapco, 2017). This meshing strategy was finely tuned with specific parameters: a prism layer thickness set to 33% to adequately resolve near-wall gradients, a volume growth rate of 1.2, and a surface growth rate of 1.3 to ensure a balanced expansion of mesh size away from critical areas, and enhanced surface control around critical surfaces set at 0.3 to maintain high resolution where flow dynamics are most complex.

2.2.3. Grid independency

In our CFD study, a crucial component was the grid independency analysis, ensuring that our simulation results were not significantly influenced by the size of the mesh used. This analysis was meticulously detailed in SI3 to transparently demonstrate the robustness of our findings against changes in mesh density.

We generated four distinct meshes, each with a progressively smaller polyhedral base size, to scrutinize the mesh's impact on the simulation's average variation in the velocity field. This step was vital in identifying an optimal mesh that offers a reliable balance between computational demand and the accuracy of the results. Throughout this analysis, we observed that the differences in simulation outcomes across all four meshes were sufficiently small to indicate good mesh independence. Crucially, the comparison between Mesh 3 and Mesh 4 revealed an

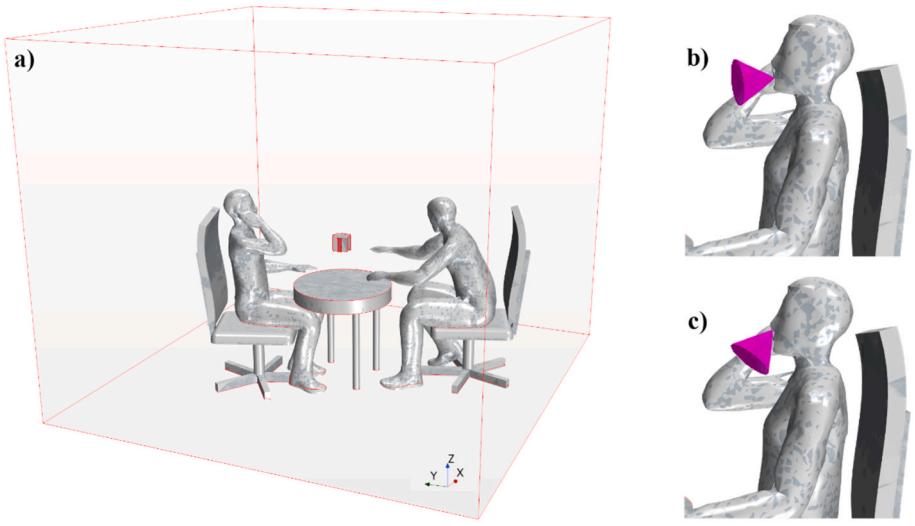

Fig. 2. a) Full control volume analyzed through CFD simulation; b) and c) the position and method of embedding particle injectors as a representative of the oral and nasal outlet of the respiratory tract in the simulation.

especially minimal difference, underscoring that further refinement (as seen in Mesh 4) did not yield significant improvements in simulation accuracy to warrant the additional computational resources. Therefore, Mesh 3 was chosen for our CFD analysis, representing the most effective compromise by ensuring both computational efficiency and the integrity of our results.

The diminishing deviations observed with each successive refinement underscore the adequacy of Mesh 3 for capturing the necessary physical phenomena without undue computational burden. This grid independency test forms a cornerstone of our simulation's validity, ensuring that the selected mesh density sufficiently resolves the flow field while remaining computationally feasible.

2.3. Validation of CFD

We evaluate the reliability of the CFD model through a comparison with experimental data. The validation uses an efficiency indicator (the efficiency coefficient ε) to evaluate how the CFD model's predictions agreed with the experimental data. The comparison involved two operation modes: one with the desktop fan operating and another with the fan turned off.

The efficiency ε, as reported in eq. (1), is calculated by dividing the difference (Δn) of the number of particles counted when the V-shaped air blades was functioning (n_{on}) by the number of particles counted when the device was off (n_{off}).

$$\varepsilon = \frac{\Delta n}{n_{off}} \tag{1}$$

Where $\Delta n = n_{off}\text{-}n_{on}$.

2.4. Analysis of parameters influencing the efficiency of V-shaped air blades

We performed a parametric analysis to assess the efficacy of desktop fans in different conditions, encompassing the investigation of three pivotal factors: fan location on the table, its height, and power settings (i.e., outlet air velocity).

The fan location over the table varied, moving the fan of 0.1, 0.2, and 0.3 m from the central axis connecting the scene's two subjects, keeping the z coordinate constant. We studied the influence of the height by keeping the central position on the x-y plane and changing the fan operation height a = 0.05 m, 0.15 m,0.2 m, and 0.3 m (original location). In this part, our objective was to investigate the influence of the parameter of mouth-to-device-top distance on the device's effectiveness. Rather than immediately constructing a new prototype with different lower dimensions, we chose to comprehensively analyze this parameter to understand its impact. This approach enables us to explore a range of stand heights, potentially varying from (value) to (value), based on the geometry studied. Finally, we modified the power settings by studying six different outlet velocities from 0 m/s (fan off) to 3 m/s. The particle emission rate was constant, equal to 10,000 particles per second with aforementioned size distribution, while the overall simulation duration was 6 s. Other conditions and parameters were constant for this sensitive analysis. This comprehensive parameter analysis facilitated a systematic investigation into the impact of fan location, height, and power settings on particle dispersion, yielding valuable insights into the effectiveness of desktop fans across a spectrum of conditions.

3. Results and discussion

3.1. Experimental results

We measured the total detected particles at the same susceptible subject proxy location. Size resolved particle count indicated the particle number in each size bin, i.e., as a function of the optical particle size (presented in SI6). The arithmetic mean over five different tests, each with the device on and off, determined the average number of particles. Each trial lasted 300 s, and the total particle count restarted every 30 s. Fig. 3 show the average quantity of particles for the two different testing conditions, highlighting the effect of the V-shaped air blades generator when turned on. Each graph of this figure indicates the total number of particles for each size bin as a function of time. The analysis conducted on the aerosol jet without the operating device (Fig. 3a) demonstrated the good reproducibility of the experimental setup. The particle count followed a typical time-dependent pattern consistent across the size spectrum: the highest count was recorded between 90 and 120 s, and the lowest count between 0 and 30 s.

Although using the desktop fan had a noticeable impact on test reproducibility, the comparison between Fig. 3a and b in terms of total particle count demonstrates the effectiveness of the V-shaped air blades generator in creating a safer zone. Indeed, the reduction of particles was between 70 and 80% in the optical diameter range of 0.35–0.84 μm. The highest decrease was 89% in the optical diameter range of 3–4 μm during the sampling time between 120 and 150 s. The cumulative number of particles over the full-size spectrum showed an average decrease of 78%, which we can consider as a reference value for the V-shaped air blades efficiency. In addition, in Fig. 3a, we observe the variation in particle concentration over time. Up to the 120-s mark, there is a continuous increase in particle concentration across all size bins, reaching a peak at 120 s, after which it gradually decreases and stabilizes. On the contrary, Fig. 3b illustrates the effect of the desktop fan being switched on, showing a slight increase until 120 s followed by reduction and stability, then a subsequent rise from 240 to 300 s. This latter increase might be attributed to an increase in bulk concentration, indicating the necessity for ventilation and filtration over prolonged periods. Alternatively, it could also be a result of measurement

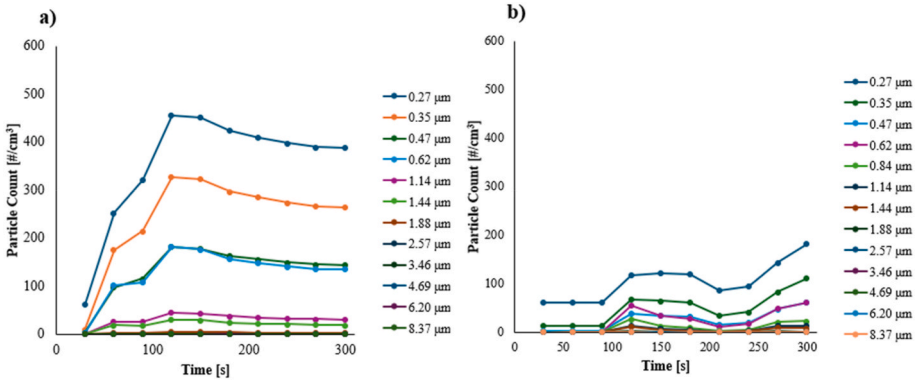

Fig. 3. Size resolved particle counts measured with OPS-3330, a) without and b) with the operation of the device generating the V-shaped air blades, over a total interval of 300 s with a 30 s timespan.

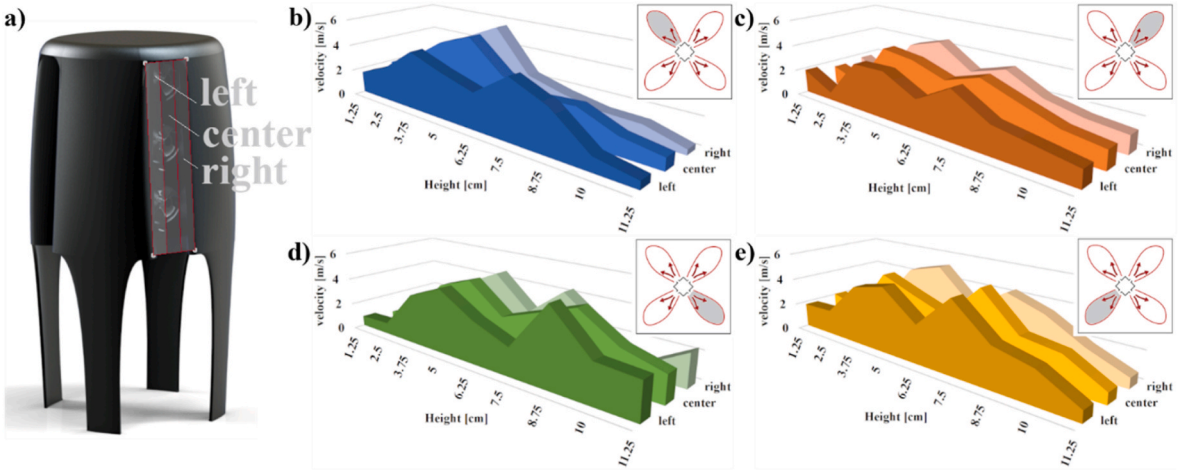

Fig. 4. a) Schematics of the vertical subdivision of the outlet section into three columns: left, center, and right. Velocity measurements were taken in each column at different heights with an interval of 12.5 mm. On the right, from b) to e), the maps show velocity profiles at the different heights for each column and four outlet sections.

fluctuations. It should be mentioned that for a detailed examination, the particle size distribution graph for the maximum time span (90–120s) and the corresponding discussions are provided in Supplementary Information (SI6), offering an opportunity for in-depth investigation.

Qualitative insights into the device operation were obtained using contrast fluoroscopy, with detailed visualizations provided in Supplementary Figure SI 6. The Supplementary Information elaborates on the observations made during the test, including the changes in droplet density and aerosol dispersion dynamics before and after device activation.

Fig. 4 presents the velocity maps obtained from the experimental assessment. For each section, the maps illustrate that the highest velocity values are concentrated in the central area, while the values at the top and bottom are relatively lower. Interestingly, there are no noticeable differences between the left, center, and right columns. The velocity measurements range from the highest value of approximately 5.5 m/s to the lowest value of around 0.7 m/s.

The exact values of the outflow velocity ranged between a minimum of 1.38 ± 0.81 m/s and a maximum of 4.58 ± 0.81 m/s, while turbulent intensity was $35.7 \pm 5.4\%$.

While small variations in velocity values exist among the different outlet sections, there is a general similarity in the trend of the curves. These velocity profiles are essential input conditions for the CFD modeling of the desktop fan in the scenario involving two individuals seated at the table in front of each other. The CFD simulations will further enhance our understanding of the air circulation dynamics and its potential influence on mitigating the transmission of airborne particles in such a gathering setting.

3.2. CFD results

The CFD simulation was configured with a fan outlet velocity, as shown in Fig. 4 and turbulence intensity reported in SI 7, with an inlet gauge pressure of 0 Pa. Dry air at 25 °C and an initial pressure of 101325 Pa are the boundary conditions for the room. We set the exhaled air plume velocity and the particle temperature to 5 m/s (Chen et al., 2020) and 37 °C, respectively (Yin et al., 2022), (Gittings et al., 2015).

Fig. 5 displays a vector (5a, 5b, 5c) and contour (5d) representation of the velocity field produced by the V-shaped air blades, respectively. These figures show the V-shaped air blades created by the desktop fan provide four distinct zones. Due to the suction and blowing created by the V-shaped air blades, turbulent flow is created in these four zones, generating reverse flow near the occupant (Fig. 5c). In addition, the magnification shows the formation of two large eddies in the respiratory area of the susceptible person (the individual depicted in a posture of talking on a mobile phone represents the infected person. Conversely, the individual seated with a slight curve in their back is identified as the susceptible person), which could change direction and return particles with low momentum. In addition, based on the velocity profile presented in this figure, it can be inferred that, due to the 90-degree distance between the blades, the velocity created by the desktop fan is not expected to exceed 0.2 m/s on the occupants' bodies, which aligns with the ANSI/ASHRAE Standard 55 (Thermal Environmental Conditions for Human Occupancy) for comfort. Furthermore, the streamlines and turbulent kinetic energy generated by the desktop fan are thoroughly discussed and depicted in detail in SI4.

To check the performance of the V-shaped air blades on the route of respiratory transmission of pathogens generated by the infective person, Fig. 5e and f show the transmission route of airborne particles in an indoor environment with and without the presence of the V-shaped air blades at different time intervals. According to results in Fig. 7e, when the V-shaped air blades is off, particles easily travel the 0.8 m interpersonal distance and enter the respiratory area of the susceptible person. Consequently, in the absence of obstacles, the vulnerable individual faces direct exposure to a viral load carried by particles of various diameters, with a significantly increased risk of infection. The particles originate as a cloud of droplets spreading after a brief distance. Finer particles stay on the original path and are still suspended in the air, while larger particles deviate from the original route. When the V-shaped air blades prototype is active (Fig. 5f), the new induced airflow pattern acts as an obstacle for the direct passage of airborne particles. The local airflow field generated by the V-shape jets alters the route of these particles, preventing them from entering a susceptible person's respiratory area.

Further, the two primary velocity fields deflect some of the particles. The second two blades mostly deflect this residue, and a very small number of particles enter the respiratory area of the vulnerable person, with a clear reduction of the infection risk.

In our study, while focusing on the effectiveness of the portable desktop fan in reducing direct exposure to exhaled aerosols, we also recognize the potential for such devices to alter the deposition patterns of these particles on nearby surfaces (fomite). For example, the enhanced local airflow created by the fan can potentially increase the number of particles settling on the table (see SI5). Thereby, despite the less relevance of fomite transmission compared to airborne risk (Jones, 2020), (Goldman, 2020) (Weber and Stilianakis, 2020), the device can elevate fomite transmission risk, highlighting the importance of regular surface cleaning and disinfection as part of a holistic approach to

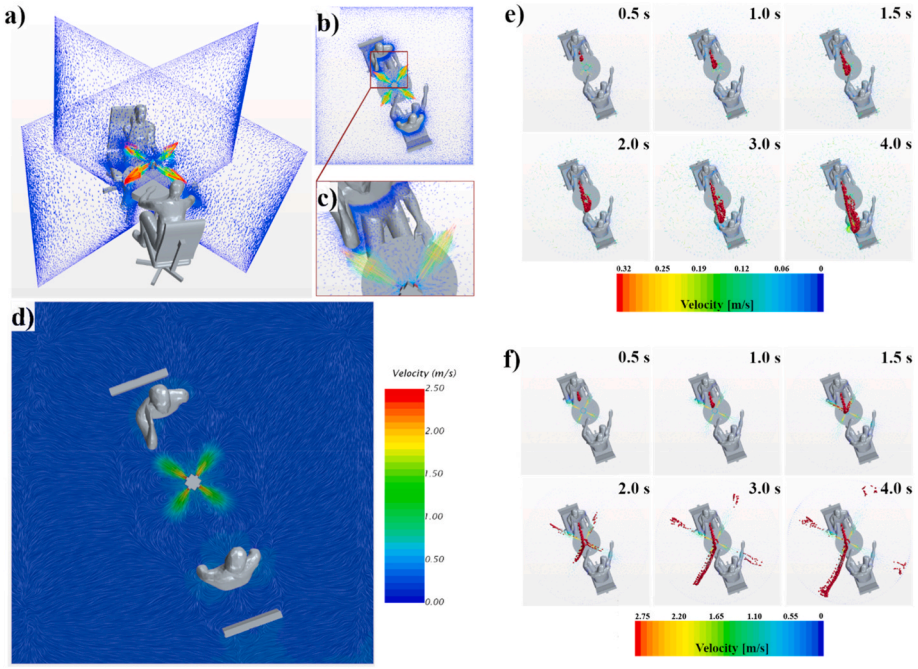

Fig. 5. Representation of velocity vectors. Image a) shows the velocity field on two vertical planes intersected with V-shaped air blades outlets. In b), c), and d), the velocity field depicts the effect of the device operation over the horizontal plane. In e) the airborne particle tracking in the closed environment without V-shaped air blades operation, while in f) Airborne particle tracking during V-shaped air blades operation.

reducing infection risks in environments where such devices are used. New studies need to investigate these aspects in multiple tables- and multiple persons-configuration.

3.3. CFD validation

The validation of the numerical model is based on the comparison between the data obtained from experimental measurements and data from the numerical simulation. The CFD simulation's test settings are listed in Table 2, and we regarded the particle emission in this simulation as being generated in a speaking mode (Cortellessa et al., 2021). The exhaled air jet speed was 5 m/s (Chen et al., 2020), assuming the number of particles produced at one time to be 1000, with the flow rate of the particles produced from two 60-degree conical injectors equal to 10000/s with the same size distribution as the previous part. In the CFD mode, the measure of particle counts considers the total number of particles reaching the surface of the nose and mouth of the susceptible person sitting at a distance of 0.8 m, as for the experimental campaign. Upon thorough examination of both experimental findings and CFD results presented in Fig. 6, it becomes apparent that the desktop fan effectively reduces the number of particles that enter the respiratory zone of individuals in close proximity. Fig. 6a and b demonstrate a consistent and proportional reduction in the particle size distribution across various size categories when the device is turned on, resulting in a stable configuration of the particle size distribution diagram. This pattern indicates the device's proficiency in maintaining a uniform decrease in particle counts. The comparison of the results in Fig. 6 demonstrates an acceptable agreement, indicating that the CFD model can be suitably used to analyze further the influence of the V-shaped air blades generator on the aerosol jet path.

Upon closer comparison of the two figures, as particle size increases the reduction in the gap between the diagrams representing data with and without the device operation (serving as an indicator of device performance) is more drastic in the case of experimental diagrams to CFD counterparts. This trend can be attributed to two primary factors. Firstly, the difference in size distribution used in the CFD simulation and experimental tests plays a significant role. Secondly, the skewed nature of the particle size distribution employed in the experimental tests contributes to this observed pattern. Specifically, the production of larger particles is notably less than that of smaller particles, creating a distribution with a bias towards smaller sizes. For instance, the particle number reaching the susceptible person without the device operation was a mere 41 for particles within the 4 to 5 μm range, while a substantial count of more than 220,000 particles was recorded within the 0.3 to 0.4 μm range. The low number of particles reduces the representativity of the results. Consequently, we acknowledge this experimental limitation and, as a result, have excluded the efficiency data for particles larger than 4 μm in the comparison of experimental results with CFD simulations.

According to this figure, our experimental results demonstrate that the portable device can effectively reduce the local concentration of aerosols in the vicinity of an infectious person by 73–89%. In contrast, CFD simulations suggest a somewhat higher reduction efficiency, ranging from 89 to 95%. Notably, within the submicron size range (<1 μm), we observed a discrepancy in reduction efficiency of less than 12% between the experimental and CFD results. This variance highlights the complexities of accurately modeling aerosol dynamics at such particle sizes. The observed differences in reduction efficiency may stem from several factors, including discrepancies in particle size distributions between the CFD and experimental setups, fluctuations in the bulk transfer of particles and increased emission rates during experimental trials, and differences in experimental and simulated boundary conditions affecting wall-particle interactions. Recognizing the significance of accurately capturing the behavior of submicron aerosols, we identify this area as a key opportunity for further refinement of our model. We aim to enhance the model's precision in simulating the dynamics of aerosols within this critical size range, thereby providing more accurate predictions of device efficacy in real-world scenarios. The ongoing effort to reconcile these differences underscores our commitment to advancing the understanding of aerosol-mediated virus transmission and the development of effective mitigation strategies.

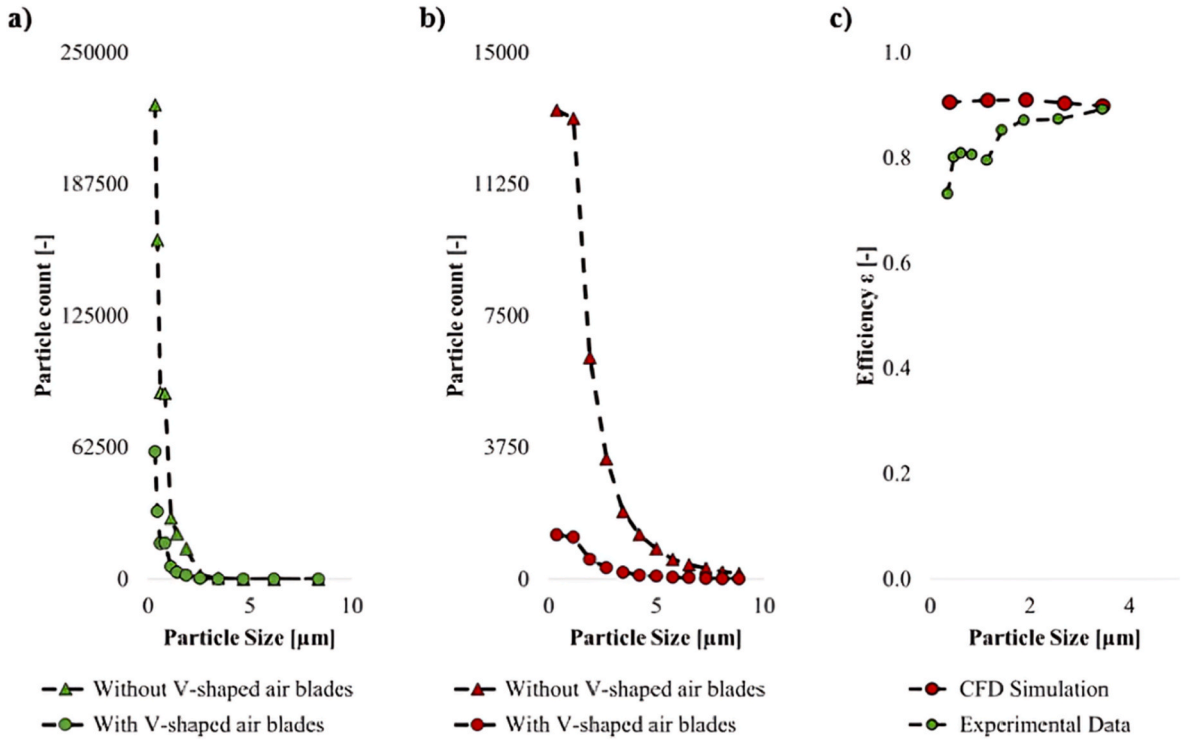

Fig. 6. Comparison of particle counts between the two testing modes (with and without the V-shaped air blades, operation over the 300 s test duration). Graph a) shows experimental results while b) the CFD results. In c) is reported the comparison of the efficiency of the V-shaped air blades between the experimental and CFD results.

3.4. Influence of fan position and power

We conducted a systematic analysis to assess the performance of the desktop fan under different conditions. We focused on three key parameters: axial deviation, height, and fan power, examining their impact on the fan's efficacy. The objective was to assess their influence on the quantity of particles conveyed from an infective source to a vulnerable individual and evaluate the efficiency of the desktop fan in mitigating the spread of exhaled airborne particles using these three parameters.

Each simulation had a duration of 6 s, and the emitter person consistently released a total of 10,000 particles per second with the previously stated size distribution. Unless explicitly specified, all parameters remained identical throughout the analysis as for the previous simulation.

3.4.1. Height

The device's height above the table is crucial to its performance. Specifically, aligning the device's height with the mouth and nose of the user can enhance its efficiency. However, it's important to note that opting for a lower height can have advantages, such as minimizing interference with eye contact and improving social interaction among individuals seated at the table. This consideration aligns with the project's design constraints, prioritizing practical acceptability in social contexts. Nevertheless, according to Fig. 7a, increasing a (lowering the height of the desktop fan from the mouth tangential level) generates a dramatic increase in the number of particles reaching the susceptible recipient. This figure further shows that the fan efficiency remains unvaried from a = 0 to a = 0.15 m. The efficiency experiences a significant decline when a increases. In particular, for finer particles (<1 μm), the efficiency drops to approximately 31%. The fan's capability to redirect particles diminishes due to alterations in local airflow dynamics and a diminished impact on particles suspended at higher levels.

3.4.2. Axial deviation

As the axial deviation increased from zero to 0.3 m, it became evident that the presence of the fan maintained its effectiveness for particles smaller than 1 μm, exhibiting an efficiency exceeding 90% for this particle size range. However, this efficacy diminished notably for larger particles, particularly those with an optical mean diameter of 1.92 μm, where the efficiency dropped to less than 30% and even more for larger particles (Fig. 7b). The decline in efficiency with increasing axial deviation, particularly for larger particles, can be ascribed to the modified airflow patterns caused by the deviation. As axial deviation rises, the fan's airflow loses effectiveness on the particle route, making it less able to redirect larger particles. We can explain this effect because larger particles possess greater inertia, making them less susceptible to the altered and less coherent airflow patterns caused by increased deviation.

3.4.3. Fan airflow

We explored a range of fan speeds to examine the effect of fan airflow on the desktop fan's effectiveness in reducing the number of particles produced by an infected individual from entering the respiratory area of a susceptible person. Reducing the fan velocity corresponds to an increase of transmitted particles. Remarkably, at a velocity of 3 m/s, near 100% efficiency is achieved by the desktop fan, whereas this efficiency declines to 37% at a velocity of 1.5 m/s, as depicted in Fig. 7c. This decrement in efficiency is markedly accentuated for a particle size <1.5 μm, whereas the fan airflow effect in the coarser size range remains comparatively unaltered.

These findings result from the complex interaction between fan-generated airflow, particle inertia, and the fan's operating height. When fan velocity decreases, its ability to capture and disperse particles diminishes, particularly affecting smaller particles more influenced by viscosity than inertia.

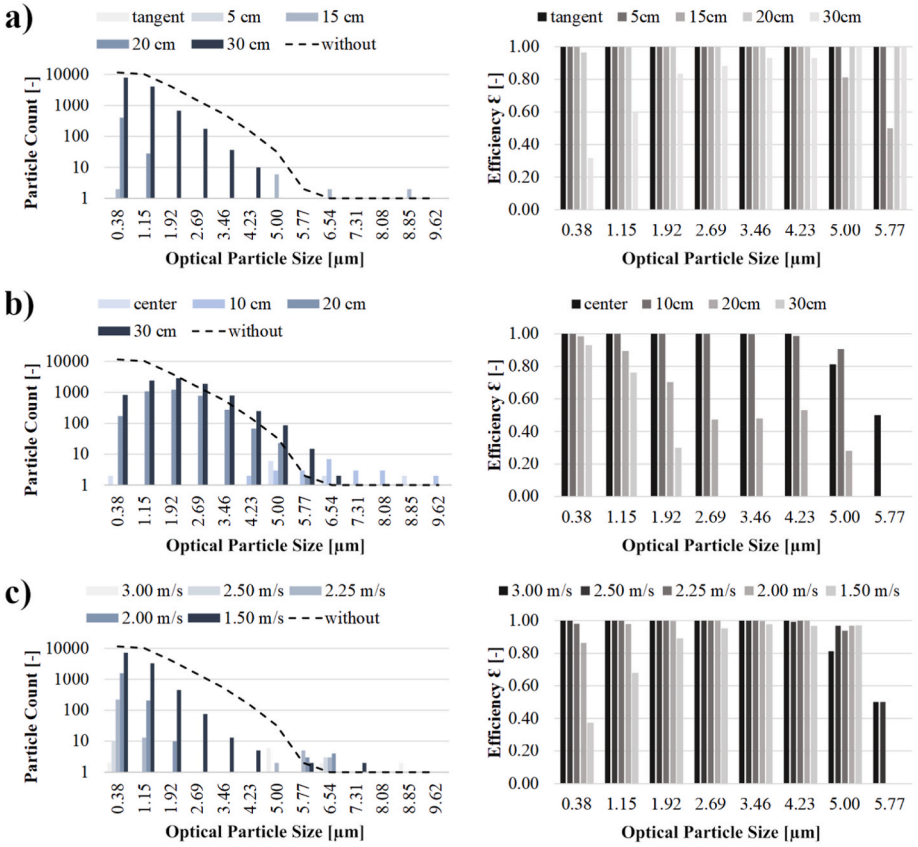

Fig. 7. Effect of a) height, b) axial deviation, and c) fan velocity on particle counting as well as V-shaped air blades effectiveness as a function of particle diameter.

4. Conclusion

We studied a cheap, portable desktop fan capable of reducing the proximity risk of contagion without cleaning the air or using outdoor air. The device generates a 90° V-shaped air blades, which acts as a barrier that can deviate and contain a potentially infected respiratory cloud, thus protecting susceptible occupants against direct exposure to airborne pathogens. The experiments used a mannequin head connected to a liquid aerosol generator on one side of a small table An optical particle sizer provided the particle size distribution that could reach the inhalation zone of a susceptible person. The CFD simulation reproduced the experimental geometry using the Eulerian-Lagrangian model. The values of device performance metric derived from the experimental data and from the numerical simulations showed a good agreement. Moreover, a parametrical analysis investigated the desktop fan's effectiveness range, using the CFD model.

The key findings are.

- according to the experimental data, the V-shaped air blades can reduce the close transmission of infective airborne particles by up to 84%.
- the CFD model showed that the V-shaped air blades induces a reversal flow in the susceptible subject respiratory zone, which may change the direction of particles and return them with low momentum.
- According to parametric analysis, the V-shaped air blades exhibited a 100% efficiency in the range of mouth tangent to −0.15 m height, 0.1 m axial deviation, and velocities exceeding 2 m/s in mitigating the dispersion of exhaled airborne particles. Furthermore, its effectiveness remained above 30% even at a height of −0.3 m, an axial deviation of 0.3 m, and velocities exceeding 1.5 m/s.

We examined the proposed device's effectiveness and efficiency as an innovative concept. The device demonstrated its effectiveness on direct exposure ("short-distance"). At the same time, the volumetric one (often called "long-distance") should be reduced by ventilation or air cleaning.

This work focused on the short-range effect of the innovative device in a single table scenario. The experimental setting was limited to a small volume with one table and focused on the local scale, excluding the accumulation of particles in the background. The CFD simulations were also limited to the same scope and some simplifications have been adopted to reduce computational time and to enable a parametrical study. The adopted assumptions were suitable for the assessment of the efficiency of the device. The results encourage to deepen the study of this device, increasing the details and considering number and size of inhaled particles. Future studies will also analyze larger rooms, multiple tables, concentration of aerosol in the indoor volume and the effect of dilution by ventilation and air cleaning for a longer duration.

CRediT authorship contribution statement

Hamed Rasam: Writing – review & editing, Writing – original draft, Visualization, Methodology, Investigation. **Vincenzo Maria Gentile:** Writing – review & editing, Writing – original draft, Visualization, Supervision, Project administration, Methodology, Investigation, Data curation, Conceptualization. **Paolo Tronville:** Writing – review & editing, Validation, Supervision, Resources. **Marco Simonetti:** Writing – review & editing, Supervision, Resources, Methodology, Investigation, Funding acquisition, Conceptualization.

Declaration of competing interest

The authors declare that they have no known competing financial interests or personal relationships that could have appeared to influence the work reported in this paper.

Data availability

Data will be made available on request.

Acknowledgments

A patent covers the V-shaped air blades device; co-authors are Mario Palazzetti, Marco Simonetti, Vincenzo Maria Gentile, Francesco Neirotti, and Luca Agnoletti; the rights owner is Politecnico di Torino. Politecnico di Torino funded the research in response to the COVID-19 emergency. The authors gratefully acknowledge the support received from Prof. Guido Saracco.

Appendix A. Supplementary data

Supplementary data to this article can be found online at https://doi.org/10.1016/j.aeaoa.2024.100263.

References

Ahmadzadeh, M., Shams, M., 2022. Multi-objective performance assessment of HVAC systems and physical barriers on COVID-19 infection transmission in a high-speed train. J. Build. Eng. 53, 104544.
Ai, Z.T., Melikov, A.K., 2018. Airborne spread of expiratory droplet nuclei between the occupants of indoor environments: a review. Indoor Air 28 (4), 500–524.
Al Assaad, D., Ghali, K., Ghaddar, N., Katramiz, E., Ghani, S., 2021. Evaluation of different personalized ventilation air terminal devices: inhalation vs. clothing-mediated exposures. Build. Environ. 192, 107637.
Anderson, E.L., Turnham, P., Griffin, J.R., Clarke, C.C., 2020. Consideration of the aerosol transmission for COVID-19 and public health. Risk Anal. 40 (5), 902–907.
Azuma, K., Yanagi, U., Kagi, N., Kim, H., Ogata, M., Hayashi, M., 2020. Environmental factors involved in SARS-CoV-2 transmission: effect and role of indoor environmental quality in the strategy for COVID-19 infection control. Environ. Health Prev. Med. 25 (1), 1–16.
Baboli, Z., et al., 2021. On the airborne transmission of SARS-CoV-2 and relationship with indoor conditions at a hospital. Atmos. Environ. 261, 118563.
Bayram, A., Korobenko, A., 2022. Modelling the transport of expelled cough particles using an Eulerian approach and the variational multiscale method. Atmos. Environ. 271, 118857.
Bhagat, R.K., Wykes, M.S.D., Dalziel, S.B., Linden, P.F., 2020. Effects of ventilation on the indoor spread of COVID-19. J. Fluid Mech. 903.
Bourouiba, L., 2020. Turbulent gas clouds and respiratory pathogen emissions: potential implications for reducing transmission of COVID-19. JAMA 323 (18), 1837–1838.
Bourouiba, L., 2021. Fluid Dynamics of Respiratory Infectious Diseases.
Burgmann, S., Janoske, U., 2021. Transmission and reduction of aerosols in classrooms using air purifier systems. Phys. Fluids 33 (3), 33321.
Cd-Adapco, S., 2017. STAR CCM+ User Guide Version 12.04, vol. 62. CD-Adapco, New York, NY, USA.
Center for Disease Control and Prevention, 2019. Healthcare Infection Control Practices Advisory Committee (HICPAC): Guidelines for Environmental Infection Control in Health-Care Facilities. U.S. Dep. Heal. Hum. Serv. Centers Dis. Control Prev., Atlanta, GA, pp. 1–235, 30329, no. July. http://www.cdc.gov/hicpac/pdf/guidelines/eic_in_hcf_03.pdf.
Chan, J.F.-W., et al., 2020. Surgical mask partition reduces the risk of noncontact transmission in a golden Syrian hamster model for coronavirus disease 2019 (COVID-19). Clin. Infect. Dis. 71 (16), 2139–2149.
Chao, C.Y., Wan, M.P., 2006. A study of the dispersion of expiratory aerosols in unidirectional downward and ceiling-return type airflows using a multiphase approach. Indoor Air 16 (4), 296–312.
Chen, C., Zhao, B., 2010. Some questions on dispersion of human exhaled droplets in ventilation room: answers from numerical investigation. Indoor Air 20 (2), 95–111.
Chen, W., Zhang, N., Wei, J., Yen, H.-L., Li, Y., 2020. Short-range airborne route dominates exposure of respiratory infection during close contact. Build. Environ. 176, 106859.
Chen, T., Cao, S.-J., Wang, J., Nizamani, A.G., Feng, Z., Kumar, P., 2021. Influences of the optimized air curtain at subway entrance to reduce the ingress of outdoor airborne particles. Energy Build. 244, 111028.
Christopherson, D.A., Yao, W.C., Lu, M., Vijayakumar, R., Sedaghat, A.R., 2020. High-efficiency particulate air filters in the era of COVID-19: function and efficacy. Otolaryngol. Neck Surg. 163 (6), 1153–1155.
Cooper, E., Milner, J., Wang, Y., Stamp, S., Mumovic, D., 2022. Modelling the impact on mortality of using portable air purifiers to reduce PM2. 5 in UK homes. Atmos. Environ. 289, 119311.
Cortellessa, G., et al., 2021. Close proximity risk assessment for SARS-CoV-2 infection. Sci. Total Environ. 794, 148749.
Cortellessa, G., Canale, C., Stabile, L., Grossi, G., Buonanno, G., Arpino, F., 2023. Effectiveness of a portable personal air cleaner in reducing the airborne transmission of respiratory pathogens. Build. Environ. 235 (January), 110222 https://doi.org/10.1016/j.buildenv.2023.110222.
Curtius, J., Granzin, M., Schrod, J., 2021. Testing mobile air purifiers in a school classroom: reducing the airborne transmission risk for SARS-CoV-2. Aerosol Sci. Technol. 55 (5), 586–599.
Eilts, S.M., Li, L., Pope, Z.C., Hogan, C.J., 2021. Characterization of exhaled particle deposition and ventilation in an indoor setting. Atmos. Environ. 262, 118602.
Gallo, O., Locatello, L.G., Mazzoni, A., Novelli, L., Annunziato, F., 2021. The central role of the nasal microenvironment in the transmission, modulation, and clinical progression of SARS-CoV-2 infection. Mucosal Immunol. 14 (2), 305–316.
Gao, N.P., Niu, J.L., 2008. Personalized ventilation for commercial aircraft cabins. J. Aircr. 45 (2), 508–512.
Gettings, J., et al., 2021. Mask use and ventilation improvements to reduce COVID-19 incidence in elementary schools—Georgia, November 16–December 11, 2020. Morb. Mortal. Wkly. Rep. 70 (21), 779.
Gittings, S., Turnbull, N., Henry, B., Roberts, C.J., Gershkovich, P., 2015. Characterisation of human saliva as a platform for oral dissolution medium development. Eur. J. Pharm. Biopharm. 91, 16–24.
Goldman, E., 2020. Exaggerated risk of transmission of COVID-19 by fomites. Lancet Infect. Dis. 20 (8), 892–893.
Grinshpun, S.A., Mainelis, G., Trunov, M., Adhikari, A., Reponen, T., Willeke, K., 2005. Evaluation of ionic air purifiers for reducing aerosol exposure in confined indoor spaces. Indoor Air 15 (4), 235–245.
Ham, S., 2020. Prevention of exposure to and spread of COVID-19 using air purifiers: challenges and concerns. Epidemiol. Health 42.
Hashimoto, Y., Yoneda, H., 2009. Numerical study on the influence of a ceiling height for displacement ventilation. In: Proceedings of the 11th International IBPSA Conference, pp. 27–30. Glasgow, Scotland, UK.
He, Q., Niu, J., Gao, N., Zhu, T., Wu, J., 2011. CFD study of exhaled droplet transmission between occupants under different ventilation strategies in a typical office room. Build. Environ. 46 (2), 397–408.
Hinds, W.C., 1999. Aerosol Technology: Properties, Behavior, and Measurement of Airborne Particles. John Wiley & Sons.
Jayaweera, M., Perera, H., Gunawardana, B., Manatunge, J., 2020. Transmission of COVID-19 virus by droplets and aerosols: a critical review on the unresolved dichotomy. Environ. Res. 188 (June), 109819 https://doi.org/10.1016/j.envres.2020.109819.
Jensen, K.A., 2020. Position paper of the Gesellschaft für Aerosolforschung on understanding the role of aerosol particles in SARS-CoV-2 infection.
Jia, W., Wei, J., Cheng, P., Wang, Q., Li, Y., 2022. Exposure and respiratory infection risk via the short-range airborne route. Build. Environ. 219 (May), 109166 https://doi.org/10.1016/j.buildenv.2022.109166.
Johnson, G.R., et al., 2011. Modality of human expired aerosol size distributions. J. Aerosol Sci. 42 (12), 839–851.
Jones, R.M., 2020. Relative contributions of transmission routes for COVID-19 among healthcare personnel providing patient care. J. Occup. Environ. Hyg. 17 (9), 408–415.
Kang, Z., Zhang, Y., Fan, H., Feng, G., 2015. Numerical simulation of coughed droplets in the air-conditioning room. Procedia Eng. 121, 114–121.
Kelly, F.J., Fussell, J.C., 2019. Improving indoor air quality, health and performance within environments where people live, travel, learn and work. Atmos. Environ. 200, 90–109.
Kulkarni, P., Baron, P.A., Willeke, K., 2011. Aerosol Measurement: Principles, Techniques, and Applications. John Wiley & Sons.
Li, C., Tang, H., 2021. Study on ventilation rates and assessment of infection risks of COVID-19 in an outpatient building. J. Build. Eng. 42, 103090.
Li, L., et al., 2022. Effect of low-cost recirculating portable air filtration on aerosol particle deposition and concentration in a conference room: experiment, theory, and simulation comparison. J. Aerosol Sci. 166, 106048.
Linden, P.F., 1999. The fluid mechanics of natural ventilation. Annu. Rev. Fluid Mech. 31 (1), 201–238.
Liu, L., Li, Y., Nielsen, P.V., Wei, J., Jensen, R.L., 2017a. Short-range airborne transmission of expiratory droplets between two people. Indoor Air 27 (2), 452–462.
Liu, L., Wei, J., Li, Y., Ooi, A., 2017b. Evaporation and dispersion of respiratory droplets from coughing. Indoor Air 27 (1), 179–190.
Liu, W., van Hooff, T., An, Y., Hu, S., Chen, C., 2020. Modeling transient particle transport in transient indoor airflow by fast fluid dynamics with the Markov chain method. Build. Environ. 186, 107323.
Ma, J., Qian, H., Liu, F., Zheng, X., 2022. Performance analysis of a novel personalized air curtain for preventing inhalation of particulate matters in industrial environments. J. Build. Eng. 58, 105014.
Mboreha, C.A., Jianhong, S., Yan, W., Zhi, S., 2022. Airflow and contaminant transport in innovative personalized ventilation systems for aircraft cabins: a numerical study. Sci. Technol. Built Environ. 28 (4), 557–574.
Melikov, A.K., 2020. COVID-19: reduction of airborne transmission needs paradigm shift in ventilation. Build. Environ. 186, 107336.
Merhi, T., Atasi, O., Coetsier, C., Lalanne, B., Roger, K., 2022. Assessing suspension and infectivity times of virus-loaded aerosols involved in airborne transmission. Proc. Natl. Acad. Sci. 119 (32).

Mikszewski, A., Stabile, L., Buonanno, G., Morawska, L., 2022. Increased close proximity airborne transmission of the SARS-CoV-2 Delta variant. Sci. Total Environ. 816, 151499 https://doi.org/10.1016/j.scitotenv.2021.151499.
Miller, S.L., et al., 2021. Transmission of SARS-CoV-2 by inhalation of respiratory aerosol in the Skagit Valley Chorale superspreading event. Indoor Air 31 (2), 314–323.
Mirzaie, M., Lakzian, E., Khan, A., Warkiani, M.E., Mahian, O., Ahmadi, G., 2021. COVID-19 spread in a classroom equipped with partition–A CFD approach. J. Hazard Mater. 420, 126587.
Morawska, L., Buonanno, G., 2021. The physics of particle formation and deposition during breathing. Nature Reviews Physics 3 (5), 300–301. https://doi.org/10.1038/s42254-021-00307-4.
Morawska, L., et al., 2009. Size distribution and sites of origin of droplets expelled from the human respiratory tract during expiratory activities. J. Aerosol Sci. 40 (3), 256–269.
Morawska, L., et al., 2020. How can airborne transmission of COVID-19 indoors be minimised? Environ. Int. 142, 105832.
Morey, P.R., 1994. Suggested guidance on prevention of microbial contamination for the next revision of ASHRAE Standard 62. Proc. IAQ'94, Eng. Indoor Environ. 139–148.
Nair, A.N., Anand, P., George, A., Mondal, N., 2022. A review of strategies and their effectiveness in reducing indoor airborne transmission and improving indoor air quality. Environ. Res. 213, 113579.
Park, S.H., Lee, K.W., Otto, E., Fissan, H., 1999. The log-normal size distribution theory of Brownian aerosol coagulation for the entire particle size range: Part I—analytical solution using the harmonic mean coagulation kernel. J. Aerosol Sci. 30 (1), 3–16.
Pistochini, T., Mande, C., Chakraborty, S., 2022. Modeling impacts of ventilation and filtration methods on energy use and airborne disease transmission in classrooms. J. Build. Eng. 57, 104840.
Ren, C., et al., 2021. Mitigating COVID-19 infection disease transmission in indoor environment using physical barriers. Sustain. Cities Soc. 74, 103175.
Ružić, D., Časnji, F., 2011. Personalized ventilation concept in mobile machinery cab. Int. J. Veh. Mech. engines Transp. Syst. 1 (37), 7–22.
Seepana, S., Lai, A.C.K., 2012. Experimental and numerical investigation of interpersonal exposure of sneezing in a full-scale chamber. Aerosol Sci. Technol. 46 (5), 485–493.
Shan, X., Zhou, J., Chang, V.W.-C., Yang, E.-H., 2016. Comparing mixing and displacement ventilation in tutorial rooms: students' thermal comfort, sick building syndromes, and short-term performance. Build. Environ. 102, 128–137.
Shao, X., Hashimoto, K., Fang, L., Melikov, A.K., Naydenov, K.G., Rasmuseen, C., 2020. Experimental study of airborne particle transmission through the doorway of a cleanroom due to the movement of a person. Build. Environ. 183, 107205.
Sheikhnejad, Y., et al., 2022. Airborne and aerosol pathogen transmission modeling of respiratory events in buildings: an overview of computational fluid dynamics. Sustain. Cities Soc. 79, 103704.
Shen, J., Kong, M., Dong, B., Birnkrant, M.J., Zhang, J., 2021. A systematic approach to estimating the effectiveness of multi-scale IAQ strategies for reducing the risk of airborne infection of SARS-CoV-2. Build. Environ. 200, 107926.
Sun, S., Li, J., Han, J., 2021. How human thermal plume influences near-human transport of respiratory droplets and airborne particles: a review. Environ. Chem. Lett. 19, 1971–1982.
Tang, J.W., et al., 2021. Dismantling myths on the airborne transmission of severe acute respiratory syndrome coronavirus-2 (SARS-CoV-2). J. Hosp. Infect. 110, 89–96.
Tobisch, A., et al., 2021. Reducing indoor particle exposure using mobile air purifiers—experimental and numerical analysis. AIP Adv. 11 (12), 125114.
V Abhijith, K., Kukadia, V., Kumar, P., 2022. Investigation of air pollution mitigation measures, ventilation, and indoor air quality at three schools in London. Atmos. Environ. 289, 119303.
Wachenfeldt, B.J., Mysen, M., Schild, P.G., 2007. Air flow rates and energy saving potential in schools with demand-controlled displacement ventilation. Energy Build. 39 (10), 1073–1079.
Weber, T.P., Stilianakis, N.I., 2020. Fomites, hands, and the transmission of respiratory viruses. J. Occup. Environ. Hyg. 18 (1), 1–3.
Wei, J., Li, Y., 2016. Airborne spread of infectious agents in the indoor environment. Am. J. Infect. Control 44 (9), S102–S108. https://doi.org/10.1016/j.ajic.2016.06.003.
World Health Organization, 2021. Roadmap to Improve and Ensure Good Indoor Ventilation in the Context of COVID-19.
Xie, X., Li, Y., Chwang, A.T.Y., Ho, P.L., Seto, W.H., 2007. How far droplets can move in indoor environments-revisiting the Wells evaporation-falling curve. Indoor Air 17 (3), 211–225.
Xu, C., et al., 2020. Effects of personalized ventilation interventions on airborne infection risk and transmission between occupants. Build. Environ. 180 (April) https://doi.org/10.1016/j.buildenv.2020.107008.
Xu, J.C., Wang, C.T., Fu, S.C., Chan, K.C., Chao, C.Y.H., 2021. Short-range bioaerosol deposition and inhalation of cough droplets and performance of personalized ventilation. Aerosol Sci. Technol. 55 (4), 474–485.
Xu, C., Liu, W., Luo, X., Huang, X., Nielsen, P.V., 2022a. Prediction and control of aerosol transmission of SARS-CoV-2 in ventilated context: from source to receptor. Sustain. Cities Soc. 76 (August 2021), 103416 https://doi.org/10.1016/j.scs.2021.103416.
Xu, J., Guo, H., Zhang, Y., Lyu, X., 2022b. Effectiveness of personalized air curtain in reducing exposure to airborne cough droplets. Build. Environ. 208, 108586.
Yang, L., Li, X., Yan, Y., Tu, J., 2018. Effects of cough-jet on airflow and contaminant transport in an airliner cabin section. J. Comput. Multiph. Flows 10 (2), 72–82.
Ye, J., Ai, Z., Zhang, C., 2021. A new possible route of airborne transmission caused by the use of a physical partition. J. Build. Eng. 44, 103420.
Yin, J., Norvihoho, L.K., Zhou, Z.-F., Chen, B., Wu, W.-T., 2022. Investigation on the evaporation and dispersion of human respiratory droplets with COVID-19 virus. Int. J. Multiph. Flow 147, 103904.
Yu, Y., et al., 2009. Contamination from electrically conductive silicone tubing during aerosol chemical analysis. Atmos. Environ. 43 (17), 2836–2839.
Yuan, X., Chen, Q., Glicksman, L.R., 1998. A critical review of displacement ventilation. ASHRAE Trans. Soc. Heat. Refrig. Airconditioning Engin 104 (1), 78–90.
Zhang, Y., et al., 2020. The impact of air change rate on the air quality of surgical microenvironment in an operating room with mixing ventilation. J. Build. Eng. 32, 101770.
Zhao, B., Liu, Y., Chen, C., 2020. Air purifiers: a supplementary measure to remove airborne SARS-CoV-2. Build. Environ. 177, 106918.
"RESIDENTIAL AIR CLEANERS A Technical "RESIDENTIAL AIR CLEANERS A Technical Summary- 3rd Edition Portable Air Cleaners Furnace and HVAC Filters." https://www.epa.gov/sites/default/files/2018-07/documents/residential_air_cleaners_-_a_technical_summary_3rd_edition.pdf (accessed Nov. 15, 2023).